Directly Measuring Atmospheric Turbulence Parameters Using Coherent Doppler Wind Lidar

Jinhong Xian[1,2], Chao Lu[2], Xiaoling Lin[2], Honglong Yang[2], Ning Zhang[1], Li Zhang[2]

[1] School of Atmospheric Sciences, Nanjing University, Nanjing 210023, China
[2] Shenzhen National Climate Observatory, Meteorological Bureau of Shenzhen Municipality, Shenzhen 518040, China

Correspondence to: Honglong Yang (yanghonglong@weather.sz.gov.cn); Ning Zhang (ningzhang@nju.edu.cn)

Abstract. Atmospheric turbulence parameters, such as turbulent kinetic energy and dissipation rate, are of great significance in weather prediction, meteorological disasters, and forecasting. Due to the lack of ideal direct detection methods, traditional structure function methods are mainly based on Kolmogorov's assumption of local isotropic turbulence and the well-known −5/3 power law within the inertial subrange, which limits their application. Here, we propose a method for directly measuring atmospheric turbulence parameters using coherent Doppler wind lidar, which can directly obtain atmospheric turbulence parameters and vertical structural features, breaking the limitations of traditional methods. The first published spatiotemporal distribution map of the power-law exponent of the inertial subrange is provided in this study, which indicates the heterogeneity of atmospheric turbulence at different altitudes, and also indicates that the power-law exponent at high altitudes does not fully comply with the −5/3 power law, proving the superiority of our method. We analyze the results under different weather conditions, indicating that the method still holds. The turbulent kinetic energy and power-law index obtained by this method are continuously compared with the results obtained with an ultrasonic anemometer for a month-long period. The results of the two have high consistency and correlation, verifying the accuracy and applicability of the proposed method. The proposed method has great significance in studying the vertical structural characteristics of atmospheric turbulence.

1 Introduction

Turbulence is the main form of motion in the atmospheric boundary layer. It plays a major role in the transportation and exchange of momentum, heat, water vapor, and matter between the surface of the Earth and the atmosphere, directly affecting human life and production activities and playing a crucial role in atmospheric motion and weather evolution (Byzova et al., 1989; Stull, 1988; Gottschall and Peinke, 2008). At present, there are still many difficulties related to the study of turbulence, and addressing them requires improvements in observational technology. Therefore, the development of atmospheric turbulence detection technology can strengthen our understanding of atmospheric turbulent motion and accelerate the development of atmospheric turbulence theory. In atmospheric modelling in particular, it is of great significance to obtain the relevant parameters and structural characteristics of atmospheric turbulence (Banakh, 2013).

In the past, there were few detection methods for measuring or inferring low-level turbulence parameters, mainly through the installation of three-dimensional ultrasonic anemometers in meteorological gradient towers (Sathe and Mann, 2013). The detection height, density, and detection

40 ability of the detectors were very limited, which hindered the development of boundary layer turbulence theory. Fortunately, with the development of remote sensing technology, as an active remote sensing device with fast response speed and three-dimensional scanning ability, coherent Doppler wind lidar has gradually become the main means of obtaining low-level atmospheric turbulence intensity (Mann et al., 2010; Choukulkar et al., 2017; Bonin et al., 2017; Bonin et al., 2016; Jin et al., 2022; Smalikho et al.,

45 2005; Branlard et al., 2013; Banakh et al., 2021; O'connor et al., 2010). However, various parameters related to atmospheric turbulence, such as turbulent kinetic energy and dissipation rate, cannot be directly observed.

According to Kolmogorov's theory of local homogeneity and isotropy, the structure function can only be determined by the kinetic energy dissipation rate (Kolmogorov, 1941; Kolmogorov, 1991).

50 Therefore, the structure function can be calculated based on the wind speed fluctuation term, and the kinetic energy dissipation rate can in turn be estimated based on the relationship between the structure function and the kinetic energy dissipation rate given by the turbulence statistical model (Sathe and Mann, 2013). In 2002, Frehlich et al. obtained the spatial statistical characteristics of a simulated turbulent velocity field using radial velocity estimation from coherent Doppler lidar data, and subsequently

55 calculated the turbulent energy dissipation rate (Frehlich and Cornman, 2002). In 2005, Smalikho et al. used coherent wind lidar to invert atmospheric turbulence parameters with two methods, i.e., the Doppler spectral width and height structure function, using the range height indicator (RHI) scanning mode. The experimental results were numerically simulated, which confirmed the reliability of these two methods (Smalikho et al., 2005). In 2008, Frehlich obtained turbulence parameters in the boundary layer using

60 longitudinal and transverse structure function methods in the plane position indicator (PPI) scanning mode with fixed pitch angle and changing azimuth angle (Frehlich and Kelley, 2008). The inversion results were compared with the detection results of ultrasonic anemometers, and the data consistency was good. In 2012, Chan et al. divided radial wind field data into subsectors under the PPI scanning mode and calculated the turbulence dissipation rate within each subsector using velocity structure

65 functions, thus obtaining the spatial distribution of the turbulence dissipation rate (Chan and Lee, 2012). In 2017, Smalikho and Banakh used the azimuth structure function in the velocity azimuth display (VAD) scanning mode to invert atmospheric turbulence parameters, and extended the applicability of this method from the convective boundary layer to the stable boundary layer (Smalikho and Banakh, 2017). From 2017 to 2019, Zhai et al. studied the vertical structure characteristics of turbulence in the

70 atmospheric boundary layer using various lidar observation models such as the VAD, PPI, and RHI (Zhai et al., 2017). They analyzed interaction characteristics between a wind turbine wake and atmospheric turbulence under the influence of underlying surfaces with different roughness, and explored the influence of atmospheric turbulence on the evolution process of aircraft wake vortices. In 2023, Wang et al. used shipborne coherent Doppler lidar to measure the energy dissipation rate and wind shear intensity

75 of turbulent flows at sea based on the structure function method, achieving the classification of turbulent mixing sources (Wang et al., 2023).

Due to the extremely complex turbulence in the atmospheric boundary layer, the assumptions of isotropy and the −5/3 power law are more realistic in the near surface layer of the atmosphere, but may not fully hold true in some complex terrains or high altitudes. Panofsky et al. specifically observed

80 various turbulence structures under complex terrain conditions and found that different terrain conditions have different turbulence energy spectral characteristics (Panofsky et al., 1982). The study by Chellale et al. also indicates that the characteristics of turbulent energy spectra are influenced by factors such as terrain and spatial location (Chellali et al., 2010). The current methods of measuring atmospheric turbulence parameters using wind lidar data based on Kolmogorov's assumption of local isotropic

85 turbulence and the well-known –5/3 power law are indirect, which have limited applicability and cannot produce accurate turbulence processes. Therefore, the aim of this study is to find a more direct method for obtaining atmospheric turbulence parameters from the perspective of spectral analysis, without the assumptions of local isotropic turbulence and the −5/3 power law. In Section 2, we introduce the instruments and data quality control methods. In Section 3, we presented the obtained turbulence spectra

90 and propose a method for directly obtaining atmospheric turbulence parameters using coherent Doppler wind lidar data. On this basis, we study the vertical characteristics of atmospheric turbulence obtained from wind lidar data and compare them with the results from three-dimensional ultrasonic anemometers to verify their accuracy, as shown in Section 4. The main conclusions of this study are presented in Section 5.

95 **2 Instruments and Data Quality Control**

The Shenzhen Shiyan Observation Base (113.90586 °E, 22.65562 °N) has a 356 m high meteorological gradient observation tower, which is the tallest in Asia (Zhou et al., 2023). The surrounding terrain and landforms of the observation tower are shown in Figure 1(a), and Figure 1(b) shows the wind lidar instrument beneath the gradient observation tower. A three-dimensional ultrasonic anemometer (CSAT3,

100 Campbell Scientific, Utah, USA) is installed at a height of 320 m on the gradient observation tower. From Figure 1, it can be seen that there are no large obstacles (such as tall buildings) around the tower. Located 1–2 km northeast of the tower there is farmland, while tall buildings are located in distant suburbs. The terrain to the south and northwest of the gradient tower is generally flat, almost completely covered by forests and lakes. Due to its excellent geographical location with no obstructions around it,

105 the monitored data are highly representative. We used wind lidar data and data obtained with the three-dimensional ultrasonic anemometer in this study. The sampling frequency of the ultrasonic anemometer is 10 Hz, and the wind speed accuracy can reach 0.1 m/s. The wind lidar (DSL-W, Darsunlaser Technology Co., Ltd., Shenzhen, China) detects a blind spot of 30 m, with a maximum detection height of 3 km and a vertical resolution of 30 m. Its time resolution is 5 s, which means its observational

110 frequency is 0.2 Hz. Specific performance indicators of the wind lidar instrument and three-dimensional ultrasonic anemometer are shown in Table 1.

The values of turbulence parameters are extremely dependent on the precision of wind speed measurements, using obtained as a time series, and the presence of too many abnormal signals can lead to the inference of abnormal turbulence parameters. Therefore, it is necessary to conduct data quality

115 control to ensure the reliability of the observed data. For the wind lidar data, an overall inspection was

conducted on the wind speed measurements every 30 min every day, eliminating data with wind speed measurements deviating from the average by more than three standard deviations (Qiu et al., 2023). For a single wind speed profile data set, if more than 20% of the data points were lost below 500 m, the entire profile was discarded. For the three-dimensional ultrasonic wind speed data, we calculated the average

120 and standard deviation of the observed values within 30 min, and any observed values deviating from the average by more than three times the standard deviation were marked as abnormal data and assigned as missing values. We repeated the above vetting process three times. During processing, data interpolation was not performed. If the number of missing measurements exceeded 20% within 30 min, the data were discarded. In order to eliminate wind speed errors caused by an installation tilt error of the

125 ultrasonic anemometer, it was necessary to rotate the coordinates of the wind speed; here, we corrected the coordinate axis using the double rotation method (Zhou et al., 2023).
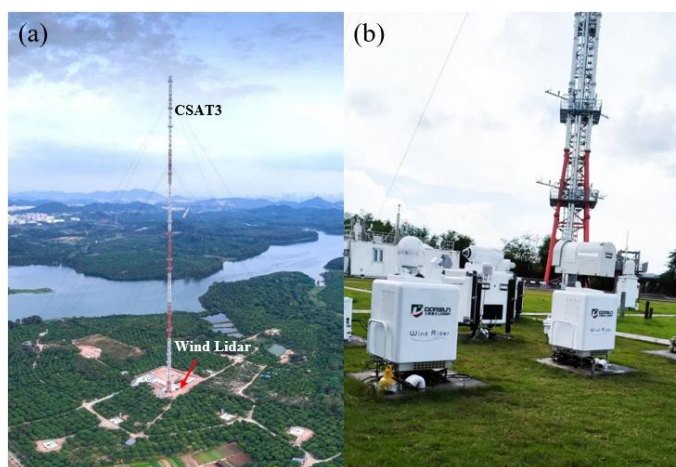
Figure 1. Topographic map of the surrounding area of the meteorological gradient observation tower (a) and installation diagram of the wind lidar below the tower (b).

130 **Table 1.** Performance parameters of the ultrasonic anemometer and wind lidar instrument

	Metrics	Technical Performance Requirements
Ultrasonic anemometer	Sample frequency	10Hz/0.1 s
	Resolution of wind speed	$\leq$0.1 m/s
	Resolution of wind direction	$\leq$1°
	Range of wind speed measurement	0–40 m/s
Wind Lidar	Minimum detection altitude	$\leq$30 m
	Maximum detection altitude	3 km
	Distance resolution	15 m
	Temporal resolution of wind profile	0.2Hz / 5 s
	Resolution of wind speed	$\leq$0.1 m/s
	Resolution of wind direction	$\leq$1°
	Range of wind speed measurement	0–60 m/s
	Range of wind direction measurement	0°– 360°

3 Methodology

3.1 Theory

The three-dimensional wind speed measured by the wind lidar and ultrasonic anemometers can be represented as $U(z, t)$, $V(z, t)$, and $W(z, t)$; where U is the east–west direction, V is the north–south direction, W is the vertical direction, z is the height, and t is the time. For the ultrasonic anemometer used in this study, z is equal to 320 m. Fast Fourier transform (FFT) calculations are performed on the wind speed within a certain time range at a certain height, z, to obtain the turbulence power spectrum, S, as

$$S_z(f) = \alpha \varepsilon^{-\frac{2}{3}} f^n,\tag{1}$$

where f is the frequency, α is the Kolmogorov constant, ε is the dissipation rate, and n is the power-law exponent. It is generally believed that $n = -5/3$ (Kolmogorov, 1991). In this study, it is considered a variable.

By taking the logarithm of both sides of Equation (1) we get

$$\log(S_z(f)) = \log(\alpha \varepsilon^{-\frac{2}{3}}) + n \log(f).\tag{2}$$

According to Equation (2), we set

$$x = \log(f),\tag{3}$$

$$b = \log(\alpha \varepsilon^{-\frac{2}{3}}),\tag{4}$$

which are substituted into Equation (2) to yield

$$\log(S_z(f)) = b + nx.\tag{5}$$

The slope can be obtained by performing linear fitting on x and $\log(S_z(f))$, which yields the power-law exponent n. The turbulent kinetic energy, κ, in a certain frequency range can be obtained by adding $S_z(f)$. When κ and n are known, the dissipation rate can be obtained from Equation (1). Therefore, this paper mainly discusses turbulent kinetic energy, κ, and the power-law exponent, n.

3.2 Method

Compared with traditional structure function methods that rely on the assumption of isotropy and the −5/3 power law, we propose a method based on spectral analysis to obtain the turbulence parameters directly. From the perspective of spectral analysis, it is possible to have a simpler and clearer understanding of atmospheric motion at different scales and types, with wider applicability and more representative significance. The scale range of vortex motion in the atmosphere is very wide, making it difficult to obtain a full frequency spectral distribution function. Usually, based on the nature of the problem being studied, the required scale range and total sampling time of the corresponding turbulent vortices are determined. For example, when studying the contribution of thermal convection or gravitational internal waves to energy in the boundary layer atmosphere, the total sampling time cannot be less than 1 h, as detection data are required to reflect vortex motion on a timescale of 10 min (Zeng et al., 2010). When studying the contribution of turbulence to energy in the inertial subrange, the total

165 sampling time usually takes 20 min, and the corresponding vortex scale ranges from a few seconds to several tens of seconds. In discrete FFT, 2^N data points are required, where N is an integer. Therefore, in this paper, we conducted FFT calculations for $2^8 \times 5$ s points (i.e., approximately 20 min) using the data obtained from the wind lidar and $2^{14} \times 0.1$ s points (i.e., approximately 27 min) for the data obtained with the ultrasonic anemometer. According to the Nyquist sampling law, the highest frequencies of turbulence

170 spectra that can be monitored by ultrasonic anemometers and wind lidar are 5 Hz and 0.1 Hz, respectively.

Figure 2 shows a comparison of turbulence spectra in the three directions (U, V, W) obtained with the wind lidar and ultrasonic anemometer, which were measured at heights of 330 m and 320 m, respectively. From the graph we can see that in all three directions the spectra have high consistency and are in good compliance with the −5/3 power law. This proves that wind lidar can effectively monitor the

175 turbulence spectrum of wind within the frequency range of $10^{-2.5}$ to 10^{-1} Hz. Based on the method proposed in Section 3.1, the turbulent kinetic energy and power-law exponent within this frequency range were obtained. Compared with structure function methods, the method of directly obtaining turbulence parameters from the perspective of spectral analysis using wind lidar does not require the assumption of isotropy and the −5/3 power law, which theoretically has higher applicability and accuracy. We verify

180 the applicability and accuracy of this method in the next section.
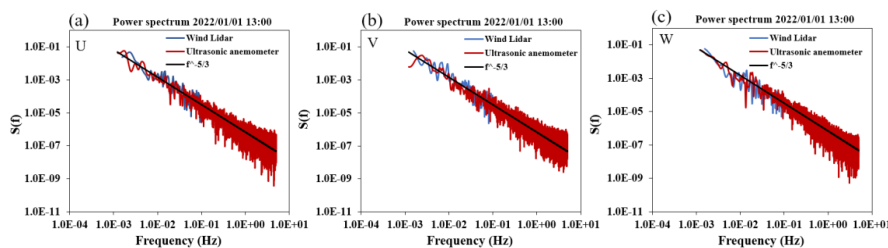
Figure 2. Comparison of the turbulence spectra obtained with the wind lidar and the ultrasonic anemometer in three directions: (a) U, (b) V, and (c) W.

4 Results and Discussion

4.1 Detection Performance under Weak Convection

Using the method proposed in Section 3.2, based on the high-resolution wind lidar data, we obtained the kinetic energy and power-law exponent at different heights; here a height of 330 m was selected as an example and the results are compared with those obtained with the three-dimensional ultrasonic

190 anemometer. Figure 3 shows a comparison of the turbulent kinetic energy obtained by wind lidar and the three-dimensional ultrasonic anemometer on 2022 January 1. The weather on that date was clear and cloudless, with an average temperature of 14 °C. The main wind direction was easterly, with an average wind speed of ~3 m/s. From the graph, it can be seen that the results of both in all three directions are relatively consistent, verifying the accuracy of wind lidar in monitoring the vertical characteristics of

195 atmospheric turbulence.

On this basis, we produced spatiotemporal distribution maps of the turbulent kinetic energy and power-law exponent, as shown in Figure 4, where panels (a)–(c) correspond to wind speed components

U, *V*, and *W*, respectively. In our model we do not assume the −5/3 power law, but instead allow it to be
a free parameter. Thus, we also present a spatiotemporal distribution map of the power-law exponent of

200 the inertial subrange in the three directions in Figures 4(d)–(f). We can observe the vertical structure and
characteristic of turbulence in Figure 4. From Figures 4(a)–(c), it can be seen that the kinetic energy in the
U and *V* directions was relatively consistent near the ground surface, but significant differences are
seen at high altitudes, such as between 18:00 and 24:00 (local time). The turbulent kinetic energy in the
W direction was relatively small because compared to the horizontal wind speed, the vertical wind speed

205 was relatively small. From Figures 4(d)–(f) it can be seen that the power-law exponent in the *U* and *V*
directions was relatively consistent most of the time, which is more in line with isotropic theory. However,
at high altitudes at night there were significant differences, where the power-law exponent in the vertical
direction (*W*) showed a phenomenon of being high at night and low during the day. This is because the
vertical wind speed is mainly driven by ground heating radiation during the day. At night, due to a lack

210 of light, the kinetic energy in the vertical direction is suppressed and the power-law exponent increases.
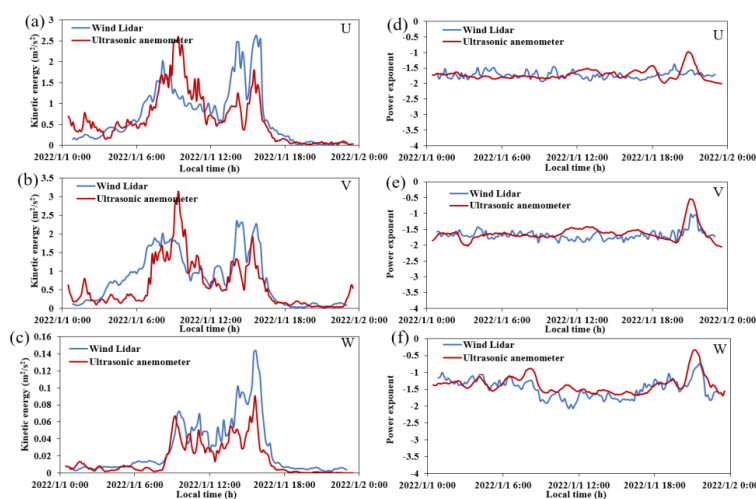
Figure 3. Comparison of the turbulent kinetic energy obtained from the wind lidar and three-dimensional ultrasonic
anemometer on 2022 January 1 in the (a) *U*, (b) *V*, and (c) *W* directions and the power-law exponent distribution in
215 the (d) *U*, (e) *V*, and (f) *W* directions.
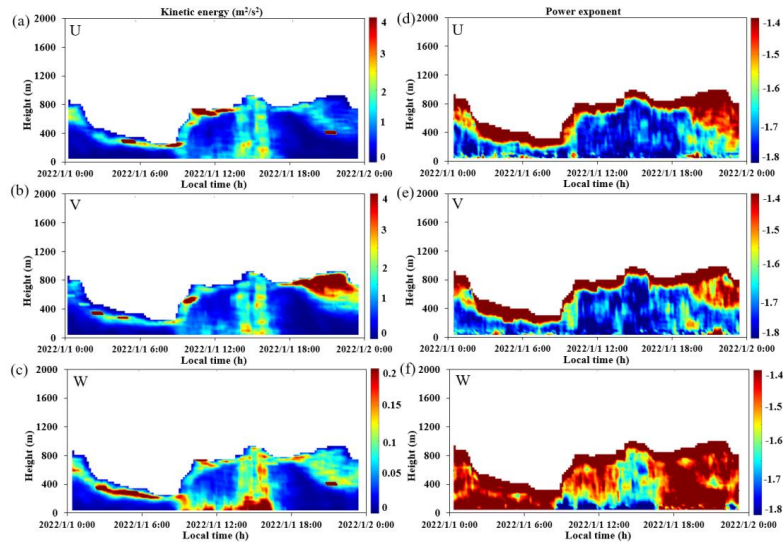
Figure 4. Temporal and spatial variations of the turbulent kinetic energy on 2022 January 1 in the (a) *U*, (b) *V*, and (c) *W* directions and the power-law exponent distribution in the (d) *U*, (e) *V*, and (f) *W* directions.

Furthermore, we present the derived power-law exponent profile in the three different directions at
220   different local times on 2022 January 1 in Figure 5. From the graph it can be seen that the power-law
exponent changed similarly in the *U* and *V* directions with height. From Figure 5(a) it can be seen that at
altitudes ~600–800 m, the turbulence in all three directions conformed to the assumptions of
homogeneity and isotropy, while at other altitudes, the turbulence in all three directions was anisotropic.
As the height increased, the power-law exponents in all three directions increased, corresponding to the
225   power-law exponent distributions shown in Figures 4(d)–(f), where there was a layer with a higher
power-law exponent, indicating the presence of kinetic energy suppression at the top of the boundary
layer. Both Figure 4 and Figure 5 intuitively and clearly reflect that the atmosphere was not isotropic and
the power-law exponent was not entirely −5/3, indicating that the atmospheric turbulence parameters
obtained by the spectral analysis method proposed in this study are more in line with the actual
230   atmospheric conditions and therefore have good accuracy.
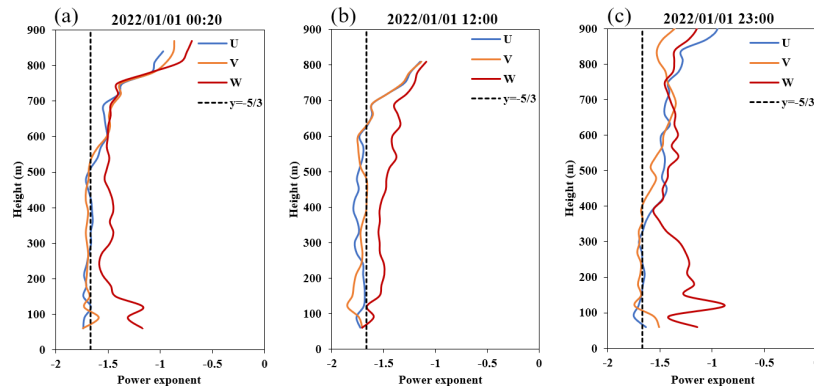
Figure 5. Power-law exponent profile of the wind speed in different directions with altitude on 2022 January 1 at (a) 00:20, (b) 12:00, and (c) 23:00 local time.

4.2 Detection Performance under Strong Convection

235   To verify the effectiveness of the proposed method under different weather conditions, Figure 6 shows the spatiotemporal variations of the turbulent kinetic energy and the power-law exponent on 2022 September 11. The weather on this day was clear and cloudless, with an average temperature of 27 °C. The main wind direction was southwest, with an average wind speed of about ~3 m/s. From the graph it can be seen that the convection was stronger on this day, with a boundary layer height of about 2000 m.

240   The turbulent kinetic energy in the U and V directions exhibited significant differences at different altitudes. The power-law exponent was relatively consistent most of the time, more in line with the assumption of isotropy, but exhibited significant differences near the ground at night. This may be due to daytime heating radiation resulting in more homogeneous atmospheric mixing, which is more in line with the isotropic hypothesis. The power-law exponent in the vertical direction (W) also showed a

245   phenomenon of high at night and low during the day. Similarly, the turbulent kinetic energy and power-law exponent at a height of 330 m were selected and compared with the results from the three-dimensional ultrasonic anemometer, as shown in Figure 7. From the graph, it can be seen that the results of both in all three directions are relatively consistent, further verifying the accuracy and applicability of wind lidar in monitoring the vertical characteristics of atmospheric turbulence.

250
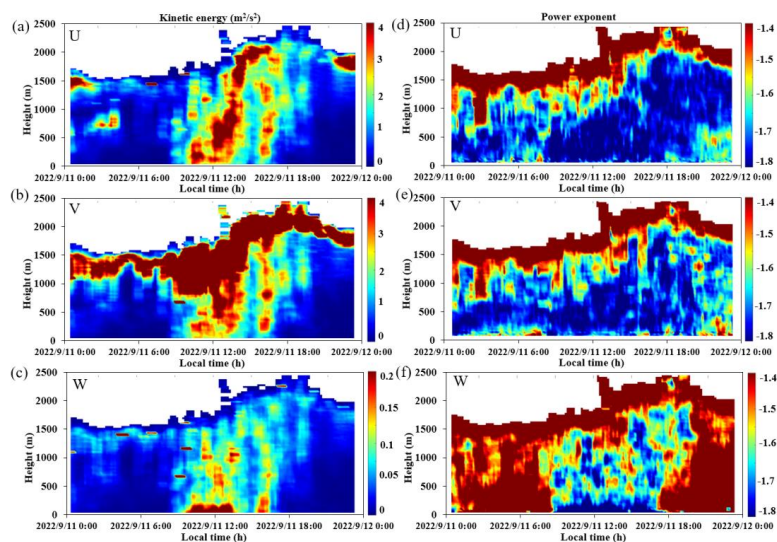
Figure 6. Temporal and spatial variations of the turbulent kinetic energy on 2022 September 11 in the (a) U, (b) V, and (c) W directions and the power-law exponent distribution in the (d) U, (e) V, and (f) W directions.
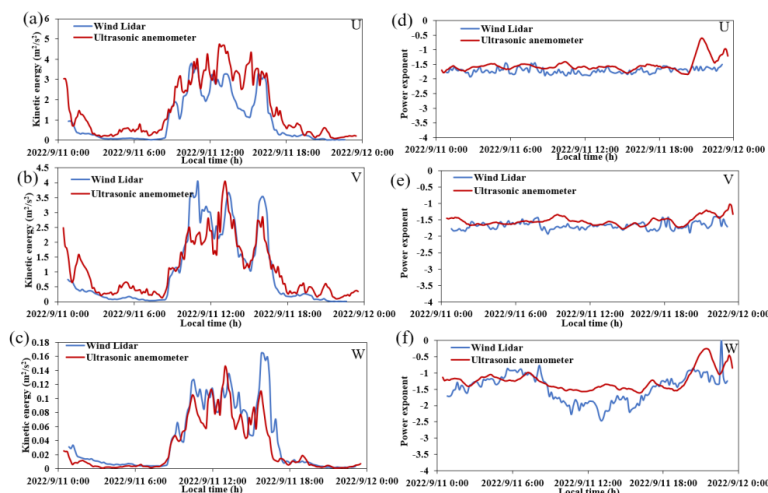
Figure 7. Comparison of the turbulent kinetic energy obtained by the wind lidar and three-dimensional ultrasonic anemometer on 2022 September 11 in the (a) *U*, (b) *V*, and (c) *W* directions and the power-law exponent distribution in the (d) *U*, (e) *V*, and (f) *W* directions.

4.3 Detection Performance in Cloudy Weather

Figure 8 shows the spatiotemporal variations of the turbulent kinetic energy and power-law exponent on 2022 January 14. On that day the weather was cloudy, with an average temperature of 13 °C. The main wind direction was easterly, with an average wind speed of 6 m/s. Similar to the previous results, the power-law exponent in the *U* and *V* directions was relatively consistent, in line with the assumption of isotropy. The power-law exponent in the vertical direction (*W*) was mainly affected by surface temperature radiation. Due to the cover of clouds during the day, the difference in the surface temperature radiation between day and night was not significant, so the phenomenon of a higher power-law exponent at night and a lower exponent during the day was not obvious. Figure 9 shows a comparison of the turbulent kinetic energy obtained by wind lidar and the three-dimensional ultrasonic anemometer on the same date. From Figures 9(a)–(c) it can be seen that the turbulent kinetic energy peaked multiple times, and the results from the two methods have high consistency under complex weather conditions. This indicates that the method proposed in this study can be utilized under different weather conditions and has high applicability.
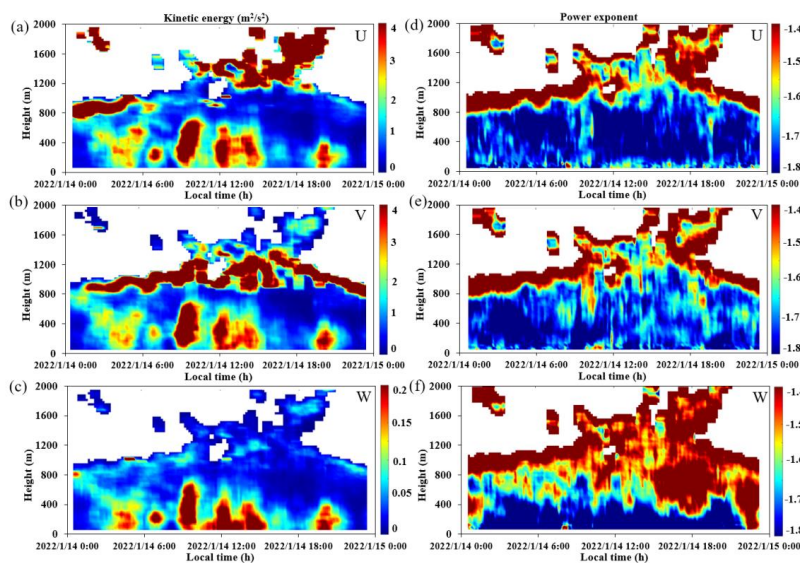
Figure 8. Temporal and spatial variations of the turbulent kinetic energy on 2022 January 14 in the (a) U, (b) V, and (c) W directions and the power-law exponent distribution in the (d) U, (e) V, and (f) W directions.
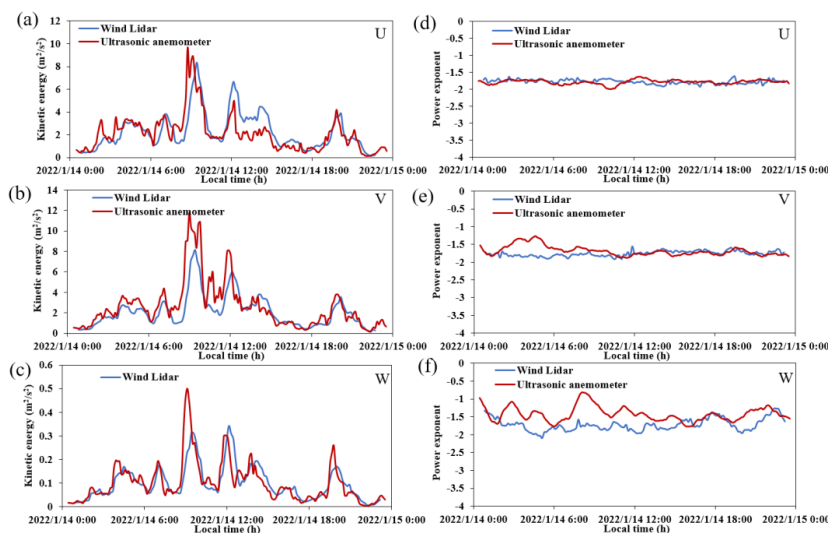
275

Figure 9. Comparison of turbulent kinetic energy obtained by the wind lidar and three-dimensional ultrasonic anemometer on 2022 January 14 in the (a) U, (b) V, and (c) W directions and the power-law exponent distribution in the (d) U, (e) V, and (f) W directions.

4.4 Continuous Long-term Verification

280   Figure 10 shows a comparison of the long-term, continuous turbulent kinetic energy obtained from the wind lidar and three-dimensional ultrasonic anemometer from 2022 January 1 to 31, where the former was measured at an altitude of 330 m. Figure 11 shows the correlation of the turbulent kinetic energy measured by the wind lidar and ultrasonic anemometer in all three directions. From the figure it can be seen that the consistency of the results is relatively good, with correlation coefficients reaching 0.91,

285 0.93, and 0.96 for the *U*, *V*, and *W* directions, respectively. Compared to the *U* and *V* components, the consistency of the comparison results in the *W* direction is the highest. This is because under different horizontal wind directions, the results of the *U* and *V* components are more susceptible to interference from the gradient tower itself, while the vertical wind speed (*W*) is not affected by this, thus yielding better results. This comparison of the continuous results indicates that the proposed method has very high

290 applicability and accuracy.
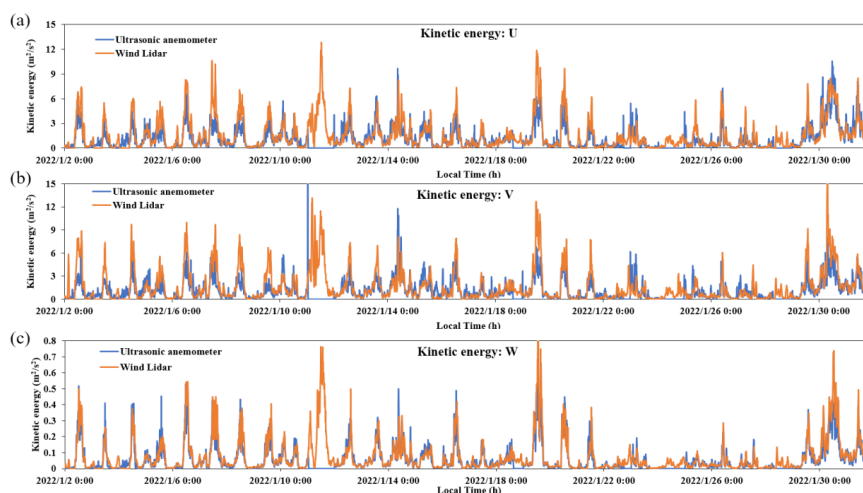
Figure 10. Comparison of the turbulent kinetic energy obtained from the wind lidar and three-dimensional ultrasonic anemometer from 2022 January 1 to 31 in the (a) *U*, (b) *V*, and (c) *W* directions.
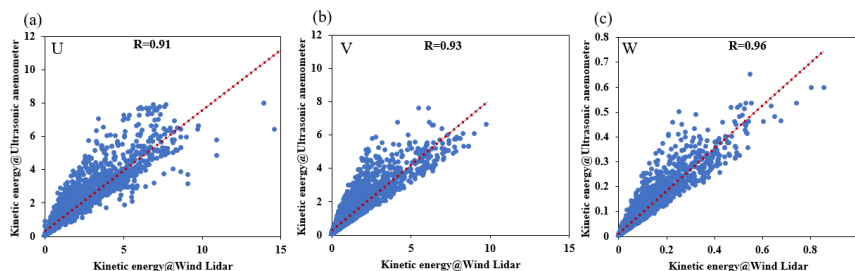
Figure 11. Correlation between the turbulent kinetic energy obtained with the wind lidar and three-dimensional ultrasonic anemometer in the (a) *U*, (b) *V*, and (c) *W* directions.

5 Conclusion

We proposed a method for directly measuring atmospheric turbulence parameters using coherent Doppler

300 wind lidar from the perspective of spectral analysis without assuming isotropy and the −5/3 power law. The method can intuitively reflect the vertical characteristics of atmospheric turbulence. In our method, the power-law index is left as a free parameter, and based on our results we have presented, for the first time, a power-law exponent spatiotemporal distribution map for the inertial subrange is provided. The results indicate that the atmosphere does not always conform to the assumption of isotropy and the −5/3

305 power law, which verifies that the proposed method of directly obtaining atmospheric turbulence

parameters from spectral analysis is more in line with the actual atmospheric conditions and has good accuracy. The obtained turbulent kinetic energy and power-law exponent were compared with the results obtained with ultrasonic anemometers for different weather conditions and over a long period (one month). The results of the three wind speed components (U, V, and W) showed good consistency, with

310   correlations reaching 0.91, 0.93, and 0.96, respectively. In complex weather conditions, there was still a high degree of consistency between the two results, indicating that the method proposed in this study has high applicability and accuracy. Compared with traditional structure function methods that rely on isotropic assumptions and the −5/3 power law, the proposed method has higher applicability and accuracy with fewer assumptions. It can obtain the spatiotemporal distributions of atmospheric

315   turbulence parameters, which have important significance in weather prediction, meteorological disasters, and forecasting.

Data availability

The data are available from the authors upon request.

Author contributions

320   Conceptualization, J.X.; methodology, J.X.; software, J.X.; validation, C.L.; formal analysis, J.X.; investigation, X.L.; resources, C.L.; data curation, L.Z.; writing—original draft preparation, J.X.; writing—review and editing, H.Y. and N.Z.; visualization, X.L.; supervision, H.Y. and N.Z.; project administration, H.Y. and N.Z.; funding acquisition, H.Y. and N.Z.

Competing interests

325   The contact author has declared that none of the authors has any competing interests.

Acknowledgements

We thank Shenzhen Darsunlaser Technology Co., Ltd.

Financial support

This work was supported by the National Key R&D Program of China (2019YFEQ124800),Special

330   Project for Sustainable Development of Shenzhen (KCXFZ20201221173412035), the National Natural Science Foundation of China (NSFC) (42275065), Guangdong Province Science and Technology Department Project (2021B1212050024), Scientific research projects of Guangdong Provincial Meteorological Bureau (GRMC2020M29), Science and Technology Innovation Team Plan of Guangdong Meteorological Bureau (GRM-CTD202003).

335 **References**

Banakh, V. A., Smalikho, I. N., Falits, A. V., and Sherstobitov, A. M.: Estimating the Parameters of Wind Turbulence from Spectra of Radial Velocity Measured by a Pulsed Doppler Lidar, Remote sensing, 13, 2071, 2021.

Banakh, V. a. S., I: Coherent Doppler Wind Lidars in a Turbulent Atmosphere, Artech House Publishers, 340 Boston, London2013.

Bonin, T. A., Newman, J. F., Klein, P. M., Chilson, P. B., and Wharton, S.: Improvement of vertical velocity statistics measured by a Doppler lidar through comparison with sonic anemometer observations, Atmospheric measurement techniques, 9, 5833-5852, 10.5194/amt-9-5833-2016, 2016.

Bonin, T. A., Choukulkar, A., Brewer, W. A., Sandberg, S. P., Weickmann, A. M., Pichugina, Y. L., 345 Banta, R. M., Oncley, S. P., and Wolfe, D. E.: Evaluation of turbulence measurement techniques from a single Doppler lidar, Atmospheric measurement techniques, 10, 3021-3039, 10.5194/amt-10-3021-2017, 2017.

Branlard, E., Pedersen, A. T., Mann, J., Angelou, N., Fischer, A., Mikkelsen, T., Harris, M., Slinger, C., and Montes, B. F.: Retrieving wind statistics from average spectrum of continuous-wave lidar, Atmos. 350 Meas. Tech., 6, 1673-1683, 10.5194/amt-6-1673-2013, 2013.

Byzova, N. L., Ivanov, V. N., and Garger, E. K.: Turbulence in Atmospheric Boundary Layer, Gidrometeoizdat, Leningrad1989.

Chan, P. W. and Lee, Y. F.: Application of Short-Range Lidar in Wind Shear Alerting, Journal of atmospheric and oceanic technology, 29, 207-220, 10.1175/JTECH-D-11-00086.1, 2012.

355 Chellali, F., Khellaf, A., and Belouchrani, A.: Application of time-frequency representation in the study of the cyclical behavior of wind speed in Algeria: wavelet transform, Stochastic Environmental Research and Risk Assessment, 24, 1233-1239, 10.1007/s00477-010-0388-x, 2010.

Choukulkar, A., Brewer, W. A., Sandberg, S. P., Weickmann, A., Bonin, T. A., Hardesty, R. M., Lundquist, J. K., Delgado, R., Iungo, G. V., Ashton, R., Debnath, M., Bianco, L., Wilczak, J. M., Oncley, 360 S., and Wolfe, D.: Evaluation of single and multiple Doppler lidar techniques to measure complex flow during the XPIA field campaign, Atmospheric measurement techniques, 10, 247-264, 10.5194/amt-10-247-2017, 2017.

Frehlich, R. and Cornman, L.: Estimating spatial velocity statistics with coherent Doppler lidar, Journal of atmospheric and oceanic technology, 19, 355-366, 10.1175/1520-0426-19.3.355, 2002.

365 Frehlich, R. and Kelley, N.: Measurements of Wind and Turbulence Profiles With Scanning Doppler Lidar for Wind Energy Applications, IEEE journal of selected topics in applied earth observations and remote sensing, 1, 42-47, 10.1109/JSTARS.2008.2001758, 2008.

Gottschall, J. and Peinke, J.: How to improve the estimation of power curves for wind turbines, Environmental research letters, 3, 10.1088/1748-9326/3/1/015005, 2008.

370 Jin, X., Song, X. Q., Yang, Y. W., Wang, M. A., Shao, S. Y., and Zheng, H. T.: Estimation of turbulence parameters in the atmospheric boundary layer of the Bohai Sea, China, by coherent Doppler lidar and mesoscale model, Optics express, 30, 13263-13277, 10.1364/OE.455079, 2022.

Kolmogorov, A. N.: Energy dissipation in locally isotropic turbulence, Dokl. Akad. Nauk SSSR, 32, 19-21, 1941.

375 Kolmogorov, A. N.: Dissipation of energy in the locally isotropic turbulence, Proc. Roy. Soc. London, 434A, 15-17, 1991.

Mann, J., Peña, A., Bingöl, F., Wagner, R., and Courtney, M. S.: Lidar Scanning of Momentum Flux in and above the Atmospheric Surface Layer, Journal of atmospheric and oceanic technology, 27, 959-976, 10.1175/2010JTECHA1389.1, 2010.

380 O'Connor, E. J., Illingworth, A. J., Brooks, I. M., Westbrook, C. D., Hogan, R. J., Davies, F., and Brooks, B. J.: A Method for Estimating the Turbulent Kinetic Energy Dissipation Rate from a Vertically Pointing Doppler Lidar, and Independent Evaluation from Balloon-Borne In Situ Measurements, Journal of atmospheric and oceanic technology, 27, 1652-1664, 10.1175/2010JTECHA1455.1, 2010.

Panofsky, H. A., Larko, D., Lipschutz, R., Stone, G., Bradley, E. F., Bowen, A. J., and Hojstrup, J.:
385 Spectra of velocity components over complex terrain, Quarterly journal of the royal meteorological society, 108, 215-230, 10.1256/smsqj.45512, 1982.

Qiu, Z. X., Xian, J. H., Yang, Y. X., Lu, C., Yang, H. L., Hu, Y. Y., Sun, J. Q., and Zhang, C. S.: Characteristics of Coastal Low-Level Jets in the Boundary Layer of the Pearl River Estuary, Journal of marine science and engineering, 11, 10.3390/jmse11061128, 2023.

390 Sathe, A. and Mann, J.: A review of turbulence measurements using ground-based wind lidars, Atmospheric measurement techniques, 6, 3147-3167, 10.5194/amt-6-3147-2013, 2013.

Smalikho, I., Köpp, F., and Rahm, S.: Measurement of atmospheric turbulence by 2-μm Doppler lidar, Journal of atmospheric and oceanic technology, 22, 1733-1747, 10.1175/JTECH1815.1, 2005.

Smalikho, I. N. and Banakh, V. A.: Measurements of wind turbulence parameters by a conically scanning
395 coherent Doppler lidar in the atmospheric boundary layer, Atmospheric measurement techniques, 10, 4191-4208, 10.5194/amt-10-4191-2017, 2017.

Stull, R. B.: An Introduction to Boundary Layer Meteorology, Springer Netherlands1988.

Wang, X. Y., Dai, G. Y., Wu, S. H., Zhu, P. Z., Li, Z. W., Song, X. Q., Zhang, S. P., Xu, J., Yin, J. P., Qin, S. G., and Wang, X. T.: Classification of Turbulent Mixing Driven Sources in Marine Atmospheric
400 Boundary Layer With Use of Shipborne Coherent Doppler Lidar Observations, Journal of geophysical research-atmospheres, 128, 10.1029/2023JD038918, 2023.

Zeng, Q. C., Cheng, X. L., Hu, F., and Peng, Z.: Gustiness and coherent structure of strong winds and their role in dust emission and entrainment, Advances in atmospheric sciences, 27, 1-13, 10.1007/s00376-009-8207-3, 2010.

405 Zhai, X. C., Wu, S. H., and Liu, B. Y.: Doppler lidar investigation of wind turbine wake characteristics and atmospheric turbulence under different surface roughness, Optics express, 25, A515-A529, 10.1364/OE.25.00A515, 2017.

Zhou, Q. J., Li, L., Chan, P. W., Cheng, X. L., Lan, C. X., Su, J. C., He, Y. Q., and Yang, H. L.: Observational Study of Wind Velocity and Structures during Supertyphoons and Convective Gales over
410 Land Based on a 356-m-High Meteorological Gradient Tower, Journal of applied meteorology and climatology, 62, 103-118, 10.1175/JAMC-D-22-0013.1, 2023.